Wireless Channel Modeling Perspectives for Ultra-Reliable Communications

Patrick C. F. Eggers, *Member, IEEE*, Marko Angjelichinoski, *Student Member, IEEE*, and Petar Popovski, *Fellow, IEEE*

***Abstract*— Ultra-reliable communication (URC) is one of the distinctive features of the upcoming 5G wireless communication, characterized by packet error rates going down to 10^{-9}. In this paper, we analyze the tail of the cumulative distribution function of block fading channels in the regime of extremely rare events, i.e., the ultra-reliable (UR) regime of operation. Our main contribution consists of providing a unified framework for statistical description of wide range of practically important wireless channel models in the UR regime of operation. Specifically, we show that the wireless channel behavior in this regime can be approximated by a simple *power law* expression, whose *exponent* and *offset* depend on the actual channel model. The unification provides a channel-agnostic tool for analyzing and performance optimization of radio systems that operate in the UR regime. Furthermore, the unified model is particularly useful in the emerging measurement campaigns for empirical characterization of wireless channels in the regime of low outages. Finally, the asymptotic analysis can serve as an underlying building block for designing more elaborate, higher-layer technologies for URC. We showcase this by applying the power law results to analyze the performance of receiver diversity schemes and obtain a new simplified expression for maximum ratio combining.**

***Index Terms*— Ultra-reliable communications, ultra-reliable low latency communication (URLLC), 5G, wireless channel models, fading, diversity, probability tail approximations, rare event statistics.**

I. Introduction

A. The Challenge of Ultra-Reliability

ONE of the features of 5G wireless communication systems is to offer service with extremely high reliability and latency guarantees, also known as *Ultra-Reliable Low Latency Communication (URLLC)* [1], [2]. The level of reliability, sometimes going down to packet error rates (PER) of 10^{-9}, as well as the unprecedented end-to-end latency requirements should be sufficiently convincing in order to remove cables in an industrial setting, remote control of robots and drones that need to perform a critical function, remote surgery or self-driving cars [3]. It is important to note that in this work we cover the aspect of ultra-reliability, but only implicitly the aspect of low latency. However, in the common 5G terminology, ultra-reliability is always coupled to low latency. We believe that this tight coupling should be relaxed, as there are scenarios in which ultra-reliability is important (e.g. health monitoring or disaster recovery), but the allowed latency can be larger than the proverbial 1 ms.

Ultra-reliability can be achieved through a combination of enabling technologies at the physical, MAC, link and the higher layers. Regardless of the techniques, an important building block of an ultra-reliable wireless system is a model of the wireless channel that captures the statistics of rare events and large fading dips. One potential application of this model is in channel training; in a related study [4] we have shown that training the channel under mismatched model, i.e., model that differs even slightly from the "ground truth" channel when the channel operates in the regime of extremely rare outages, will severely violate the reliability constraint. Another situation is the introduction of spatial diversity; without adequate understanding of the behavior of the single-antenna wireless link in regime of rare events, one cannot hope for any operational understanding of the multi-antenna links.

To the best of our knowledge, no experiments are yet being considered for reliability targets lower than 10^{-5}. Such an endeavor requires a major effort in terms of measurement campaigns and data analytics, purposefully designed to capture the lower tail statistics and extrapolate the dominant factors that determine the behavior of wireless channels in such extreme operational regime. The amount of data necessary to extrapolate such knowledge is rather massive, while the required reliability of the experimental setup is on par with space mission designs. The first step towards such experimental characterization is a statistical tool that parameterizes various channel models in the UR-regime; this is precisely the topic of this paper.

B. Our Contributions

The current channel models have been developed for wireless communication systems[1] that deal with bit error

Manuscript received January 10, 2018; revised July 28, 2018 and December 8, 2018; accepted February 12, 2019. Date of publication March 5, 2019; date of current version April 9, 2019. This work was supported in part by the European Research Council (ERC) under the European Union Horizon 2020 Research and Innovation Program, through the ERC Consolidator, under Grant 648382 WILLOW. The associate editor coordinating the review of this paper and approving it for publication was Z. Sun. *(Corresponding author: Petar Popovski.)*

P. C. F. Eggers and P. Popovski are with the Department of Electronic Systems, Aalborg University, 9220 Aalborg, Denmark (e-mail: pe@es.aau.dk; petarp@es.aau.dk).

M. Angjelichinoski was with the Department of Electronic Systems, Aalborg University, 9220 Aalborg, Denmark. He is now with the Department of Electrical and Computer Engineering, Duke University, Durham, NC 27708 USA (e-mail: maa@es.aau.dk).

Color versions of one or more of the figures in this paper are available online at http://ieeexplore.ieee.org.

Digital Object Identifier 10.1109/TWC.2019.2901788

[1]For example, the first generation digital systems, such as GSM, that had an emphasis on voice communication.

rates (BER) of 10^{-3} to 10^{-4} [10]. Moreover, the models, characterized primarily in [7], [8], [20], [21], and [24] have complicated expressions for the CDFs which, in many cases of practical interest, depend on multiple parameters. As a result, they are often too obscure, not very insightful and, most importantly, difficult to use in practice.

Our objective is to provide simplified and insightful characterization of the asymptotic behavior of common wireless channel models in operational regime which is relevant for ultra-reliable applications, relying on *first order* asymptotic tail approximations. The outcome of the analysis, which is also the central contribution of the paper is a unified framework for modeling and assessment of virtually all practically significant parametric models for wireless channels operating in the UR regime. We note that our analysis does not propose nor suggest any specific technique for achieving the ultra-reliability; rather, we simply characterize the behavior of the channel in such regime which, extracting important insights and knowledge that can be further used in the design and/or performance optimization of URLLC systems. Specifically, we focus on the packet errors that occur due to outages, induced by block fading, rather than errors caused by noise. Recent studies [9] have shown that this is a very suitable model for transmission of short packets, which are in turn expected to be prevalent in the URLLC scenarios (e.g. monitoring and remote control of processes via large sensor deployments). Such applications often sacrifice the transmission rates for highly reliable and timely delivery of short information packets; thus, the traditional objective of sum rate maximization is no longer the main objective. Throughout the paper we will use the term *UR-relevant statistics* to denote erroneous events that occur during reception with probabilities $\epsilon \leq 10^{-5}$, corresponding to the reliability of "five nines". Correspondingly, we use *UR-relevant regime* when referring to the operation regime where the performance of the system is dominated by such rare events. We have selected 10^{-5} as the "gate" of the UR-relevant regime since this is the target PER for URLLC selected in 3GPP for a packet of 32 bytes to be delivered within 1 ms [35].[2]

Our analysis shows that, despite the complicated CDFs $F(\cdot)$, the behavior of the lower tail in UR-relevant regime can be significantly simplified and, for wide variety of models (but not all), unified in the following *power law* expression:

$$F\left(\frac{P_R}{A}\right) \approx \alpha \left(\frac{P_R}{A}\right)^{\beta}, \tag{1}$$

where A is the average received power over the channel, P_R is the minimal required power at the receiver to decode the packet correctly at rate R and α, β are parameters that depend on the actual channel model. We note that (1) is an asymptotic approximation, becoming increasingly valid when the ratio between the actual power and the average received power decreases which implies low transmission rates; hence, the analysis inherently fits narrowband URLLC applications with focus on highly reliable and timely delivery of short packets rather than the actual rate. We also note that the above simple power law approximation (1) can be deduced via an approach based on extreme value theory [4]; the Pickands-Balkema-de Haan theorem in extreme value theory states that, for a large class of distributions F (i.e., those whose point of attraction is 0), there exists a constant $\beta > 0$ such that $\lim_{t\to 0} \frac{F(ty)}{F(t)} = y^{\beta}$ for every $y > 0$ and, thus, justifying (1).

In addition, we have also characterized the UR-relevant statistics when multiple antennas are considered. Specifically, we provide a simplified analysis of M-branch receive diversity for uncorrelated branch signals, that makes use of (1), as well as the corresponding approximations for some special channels that do not adhere to power law tail behavior. The result provides a compact Maximum Ratio Combing (MRC) solution of the form

$$F_{\mathrm{MRC}} \approx \alpha_{\mathrm{MRC}}(\beta_1..\beta_M) F_{\mathrm{SC}}, \tag{2}$$

that is, a scaled version of a Selection Combining (SC) solution, in which the scale parameter α_{MRC}[3] depends only on the exponents β of all M branches.

To illustrate the usefulness of our analysis, consider a simple scenario where a transmitter transmits to a receiver over flat fading wireless channel. Both the transmitter and the receiver are equipped with one antenna. The CDF of the received power is denoted with F. Assume that link outages are the dominant source of errors; in such case, the maximum rate R at which the transmitter can deliver information to the receiver, i.e., the ϵ-outage capacity is given by:

$$R_{\epsilon}(F) = \log_2(1 + F^{-1}(\epsilon)), \tag{3}$$

where $F^{-1}(\epsilon)$ denotes the ϵ-quantile of the channel distribution. The transmitter seldom knows F perfectly and in practice, specific channel estimation procedure is applied, where the channel is estimated using n channel measurements, obtained e.g. through a dedicated training phase. In conventional mobile radio, the transmitter estimates F using *all* n channel measurements, generating an estimate which is valid over the complete support of F. This traditional approach is not well fitted for URLLC systems for two reasons: 1) estimating the channel over the whole support might produce results that are highly inaccurate at the lower tail, sometimes leading to over-/under-estimation of R and severe violation of the reliability constraint, and 2) F might be dependent on many parameters, some of which are not related to the behavior of the CDF for very small ϵ and estimating all of them leads to useless overhead in URLLC applications. On the other hand, (1) gives a simple and elegant way of summarizing the lower tail behavior only via *two* parameters. However, (1) is only an asymptotic approximation; hence, in order to estimate the parameters α and β, the transmitter will use only a *small fraction* $m \ll n$ (e.g. 1%) of channel measurements with the *smallest* values. This can even further simplify and reduce the implementation cost in memory-limited designs.

Another consequence of the main result (1), still related to channel training is the following. When the channel operates

[2]Different mission-critical services will use different levels of ultra-reliability, such as PERs of 10^{-6} in smart grids and 10^{-9} for factory automation [3].

[3]Represents the additional diversity gain of MRC over SC, aiding in decision making for worthwhile diversity complexity

in UR regime, training the channel using mismatched model, i.e., model that differs from the actual channel and later on optimizing its performance using the mismatched channel, will lead to severe degradation of the realized reliability [4]. Our results provide a unified way to model the channel in UR regime without having to assume any specific channel model in advance. In addition to this, one can also use (1) to identify which channel model is the most appropriate in given circumstances.

The paper is organized as follows. After the introduction, in Section II we provide the system model. Section III contains analysis of a wide range of channel models which exhibit power law tails at UR-relevant probabilities. Section IV contains analysis of two models that do not result in power law tails. Section V contains the analysis of the receive diversity schemes in UR-relevant regime. Section VI concludes the paper.

II. Wireless Channel Modeling for UR-Relevant Statistics

A. Preliminaries

The common approach in wireless channel modeling is to assume *separability* of the following effects [12]:

- Path loss, dependent on the actual geometric setting and operating frequency.
- Long-term fading (i.e., shadowing) that captures slowly-varying macroscopic effects.
- Short-term fading processes, relevant on a time scale of a packet (i.e., quasi-static fading) or even a symbol (fast fading), assuming stationary scattering conditions.

The performance of the system in UR-relevant regime is determined by the short-term process and its (un)predictability, which ultimately determines the fate of the packet at the destination. Assuming separability, the statistics of short-term fading is described via parameters that are derived from the long-term fading and path loss effects; these parameters are assumed to be constant over a period of time. However, separability becomes problematic when UR-relevant statistics is considered, since the estimated long-term parameters require certain level of accuracy in order to have a valid short-term statistics of rare events. Motivated by this, we also consider *combined* long and short term fading models. Furthermore, in absence of dedicated URC channel models, we investigate the behavior of a wide palette of existing wireless channel models in UR-relevant regime of operation.

B. General Model

We use combination of (a) the complex baseband model of a narrowband channel with reduced wave grouping from [7], and (b) the incoherent multi-cluster channel of [16] and [18]. Let P denote the total received power; we have:

$$P=\omega\sum_{m=1}^{\mu}|V_m|^{2/\gamma},\quad V_m=\xi\left(\sum_{i=1}^{N}\rho_{i,m}e^{j\phi_{i,m}}\right)+\prod_{l=1}^{L}V_{\mathrm{dif},m,l}. \tag{4}$$

V_m denotes the complex received voltage from the $m-$th cluster $m=1,\ldots,\mu$, in which $\rho_{i,m}/\phi_{i,m}$ is the amplitude/phase of the $i-$th specular component, $i=1,\ldots,N$ and $V_{\mathrm{dif},m,l}$ is the $l-$th diffuse component for the $m-$th cluster with L denoting the number of diffuse components per cluster in a cascaded setting with L links [11]. Regarding the L, we note that in this paper we do not threat channel models with $L>2$, i.e., we only consider cases of $L=0$ (corresponding to ray-tracing channel models, such as the two-wave model and its three-wave generalization), $L=1$ which captures all remaining models except the Cascaded Rayleigh where $L=2$. γ in (4) caters for the modeling of a Weibull channel [15], and for all other models it is set to $\gamma=1$. The shadowing effects are represented by the random variables (RVs) ξ and ω. Here ξ is a common shadowing amplitude that affects only the specular components [24], while ω induces a shadowing effect on the total power [12], [21], see section III-G. We assume that each ρ_i of a specular component is constant and that ϕ_i is a uniform RV [7]. The elementary diffuse components $V_{\mathrm{dif},m,l}$ are treated in their simplest form, as a contribution from a large number of waves and application of the central limit theorem [7], [16], [18], which leads to $V_{\mathrm{dif},m,l}=X_{R,m,l}+jX_{I,m,l}$, where $X_{R,m,l}$ and $X_{I,m,l}$ are independent Gaussian variables, each with zero mean and variance ${\sigma_{m,l}}^2$. A more general variant of the diffuse component follows from a multi-scatter physical setup [11], [16], [18]. This leads to the cases of Nakagami, Weibull and Cascaded Rayleigh channel, as well as compound channels, such as Suzuki and shadowed $\kappa-\mu$ [12], [20], [21], [24].

We treat narrowband channel models with block fading, such that the power at which the packet is received remains constant and equal to P given with (4). The noise power is normalized to 1, such that P also denotes the Signal-to-Noise Ratio (SNR) at which a given packet is received. For each new packet, all RVs from (4) are independently sampled from their probability distributions.[4] The average received power for the channel model (4) is denoted by A and can be computed as:

$$A=E[P]\overset{(a)}{=}\overline{\omega}\sum_{m=1}^{\mu}\left[\overline{\xi^2}\left(\sum_{i=1}^{N}\rho_{i,m}^2\right)+E\left[\prod_{l=1}^{L}|V_{\mathrm{dif},m,l}|^2\right]\right], \tag{5}$$

with $E[\cdot]$ denoting the expectation operator. Note that (a) is valid when we treat the reduced wave grouping model from [7]. In the subsequent analysis we assume normalized shadowing power, i.e. $\overline{\omega}=E[\omega]=1$ and $\overline{\xi^2}=E[\xi^2]=1$. The diffuse term depends on link signal correlation, while for a single link ($L=1$) the average power of the elementary terms is $E[|V_{\mathrm{dif},m}|^2]=2\sigma^2$.

C. Descriptive Metrics

The specular component vector balancing in the reduced wave group model of [7] is given via the peak to average

[4]The reader may object that this assumption is not valid when long-term shadowing is treated, i.e. a sample for a given ρ_i is applicable to several packet transmissions. See Section IV-A for discussion about this assumption.

TABLE I

CDF TAIL APPROXIMATIONS $\tilde{\epsilon}$, FOR DISTRIBUTIONS IN THE FOLLOWING SUBSECTIONS. RELATIVE POWER $p = P_R/A$, GAIN OFFSET (SCALE) α AND LOG-LOG SLOPE (SHAPE) $\beta = \frac{d\log(F)}{d\log(p)}$ FOLLOWING (1)

Channel Model	Tail $\tilde{\epsilon} = \lim_{p\to 0} F(p)$	Offset α	Slope β
TW	$\frac{1}{2} - \frac{1}{\pi}\text{asin}\left(\frac{1-p}{\Delta}\right)$	$\frac{\sqrt{2}}{\pi}$ when $\Delta \to 1$	$\frac{1}{2}$
3W	$\frac{P_R}{4\pi\Delta_r}$	$\frac{1}{4\pi\Delta_r}$ when $\rho_1 < \rho_2 + \rho_3$	1
Rayl	p	1	1
Rice	$F_{\text{Rayl}}\left(p(k_1+1)\right)e^{-k_1}$	$(k_1+1)e^{-k_1}$	1
TWDP	$F_{\text{Rice}}\left(p;k_2\right)I_0\left(k_2\Delta\right)$	$(k_2+1)e^{-k_2}I_0\left(k_2\Delta\right)$	1
Wei	$(\Gamma(1+1/\gamma)p)^\gamma$	$\Gamma(1+1/\gamma)^\gamma$	γ
Nak	$(m^m/\Gamma(m+1))\,p^m$	$m^m/\Gamma(m+1)$	m
$\kappa\mu$	$F_{\text{Nak}}(p;\mu)F_{\text{Rice}}(1;\kappa)^\mu$	$\frac{\left(e^{-\kappa}(\kappa+1)\mu\right)^\mu}{\Gamma(\mu+1)}$	μ
$\kappa\mu/m$	$F_{\text{Nak}}(p;\mu)(1+\kappa)^\mu\left(\frac{m}{\kappa\mu+m}\right)^m$	$\frac{\mu^\mu(1+\kappa)^\mu}{\Gamma(\mu+1)}\left(\frac{m}{\kappa\mu+m}\right)^m$	μ
$\kappa\mu/\alpha$	$F_{\kappa\mu}(p;\kappa,\mu)\cdot\frac{\Gamma(\alpha+\mu)}{(\alpha-1)^\mu\Gamma(\alpha)}$	$\alpha_{\kappa\mu}\cdot\frac{\Gamma(\alpha+\mu)}{(\alpha-1)^\mu\Gamma(\alpha)}$	μ
Suz	$P_R 10^{\frac{1}{10}(\sigma^2_{\text{dB}}(\frac{\ln 10}{20})-\mu_{\text{dB}})}$	$10^{\frac{1}{10}(\sigma^2_{\text{dB}}(\frac{\ln 10}{20})-\mu_{\text{dB}})}$	1
Cas	$-p\frac{1+\Gamma}{1-\Gamma}\ln\left(p\frac{1+\Gamma}{(1-\Gamma)^2}\right)$	-	$1+\frac{1}{\ln(p)+\ln\frac{1+\Gamma}{(1-\Gamma)^2}}$
LN	$\frac{1}{4}e^{-\frac{\left(\frac{1}{2}\ln(P_R)-a\sigma_l-\mu_l\right)^2}{2\sigma_l^2}}$	-	$\frac{10}{\ln 10}\left[\frac{a}{\sigma_{\text{dB}}}-2\frac{P_{R,\text{dB}}-\mu_{\text{dB}}}{2\sigma^2_{\text{dB}}}\right]$

ratio of the two dominant specular powers:

$$\Delta = \frac{2\rho_1\rho_2}{\rho_1^2+\rho_2^2}. \tag{6}$$

Furthermore, for the single link channels, i.e., $L = 1$, the power ratio of the specular components and the diffuse component per cluster, called *k-factor* is defined as $k_N = \frac{\sum_{i=1}^N \rho_i^2}{2\sigma^2}$, which in case of the multiple clusters gives [18]:

$$\kappa = \frac{1}{\mu}\sum_{m=1}^{\mu} k_{N,m} = \frac{\sum_{m=1}^{\mu}\sum_{i=1}^{N}\rho_{i,m}^2}{\mu\cdot 2\sigma^2}. \tag{7}$$

D. UR-Relevant Statistics

Let R denote the transmission rate of the packet. We assume that packet errors occur due to outage only, such that the PER ϵ is given by:

$$\epsilon = \Pr(R < \log_2(1+P)) = \Pr(P < P_R), \tag{8}$$

where $P_R = 2^R - 1$ is the minimal required power to receive the packet sent at rate R. Denote by ϵ the target packet error probability (PER), also referred to as *outage probability*. Then, for each model the objective is to find P_R, defined in (8) through the CDF $F(P_R)$, obtained as:

$$\epsilon = F(P_R) = \int_{r_{\min}}^{\sqrt{P_R}} f(r)\text{d}r, \tag{9}$$

where $r = \sqrt{P}$ is the received envelope and $r_{\min}$ is the minimal value of the envelope in the support set of $f(r)$, which is the Probability Density Function (PDF) of the specific channel model. The key to the approximations presented in this paper is the fact that, for URLLC scenarios, ϵ is *very small*.

III. CHANNELS WITH POWER LAW TAIL STATISTICS

We analyze the behavior of common wireless channel models in UR-relevant regime and derive asymptotically tight approximations $\tilde{\epsilon}$ of their tail probabilities ϵ, that satisfy $\lim_{P_R\to 0}\tilde{\epsilon} = \epsilon$. The common trait of all models considered in this section is that $\tilde{\epsilon}$ takes the form of a simple power law (1), with distribution-specific values of the parameters α, β.

For the channel models that are important in practice (see subsections III-A-III-F), we also provide a simple tool to analyze the convergence of $\tilde{\epsilon}$ to ϵ. Specifically, we introduce the non-negative *approximation error function* $\phi(P_R)$ that satisfies the inequality (see Appendix A):

$$\tilde{\epsilon}(1-\phi(P_R)) \le \epsilon \le \tilde{\epsilon}(1+\phi(P_R)). \tag{10}$$

$\phi(P_R)$ increases monotonically with P_R and satisfies $\lim_{P_R\to 0}\phi(P_R) = 0$. We say that $\tilde{\epsilon}$ converges asymptotically to ϵ in the sense that $\left|\frac{\tilde{\epsilon}}{\epsilon} - 1\right| \le \eta$ if $P_R \le \phi^{-1}\left(\frac{\eta}{1+\eta}\right)$ for some small error tolerance $\eta > 0$. In other words, $\phi(P_R)$ can be used to compute the range of envelopes over which the relative tail approximation error is less than η.

Table I summarizes the tail approximations that are derived in the sequel.

A. Two-Wave Model (TW)

We start with the common Two-Wave channel model [7], where $\mu = 1$, $N = 2$ and $L = 0$, i.e., single cluster, two specular and no diffuse components. The envelope PDF is given by:

$$f_{\text{TW}}(r) = \frac{2r}{\pi A_{\text{TW}}\sqrt{\Delta^2 - \left(1-\frac{r^2}{A_{\text{TW}}}\right)^2}}, \tag{11}$$

where $A_{\text{TW}} = \rho_1^2 + \rho_2^2$, Δ is given by (6) and $r \in [r_{\min}, r_{\max}] = \left[\sqrt{A_{\text{TW}}(1-\Delta)}, \sqrt{A_{\text{TW}}(1+\Delta)}\right]$.

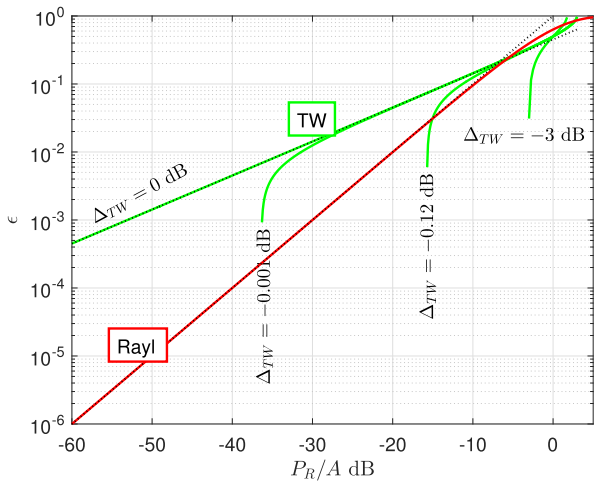

Fig. 1. Two-wave (12) and the classical Rayleigh (16) CDFs and their tail approximations (13), (17) (black dotted lines). For Two-wave: $\rho_1 = 1$, while ρ_2 is set to correspond to the Δ (6) given at each curve.

By putting $f_{\mathrm{TW}}(r)$ in (9) we obtain the CDF:

$$\epsilon = F_{\mathrm{TW}}(P_R) = \frac{1}{2} - \frac{1}{\pi}\mathrm{asin}\left(\frac{1 - \frac{P_R}{A_{\mathrm{TW}}}}{\Delta}\right). \tag{12}$$

Bounding ϵ from below leads to the tail approximation:

$$\tilde{\epsilon} = \frac{1}{\pi}\sqrt{\frac{2}{A_{\mathrm{TW}}}}\sqrt{P_R^{\star}}, \tag{13}$$

where $P_R^{\star} = \frac{1}{\Delta}P_R - \frac{1-\Delta}{\Delta}A_{\mathrm{TW}}$. The approximation error function is (see Appendix A):

$$\phi(P_R) = \frac{4}{3}\sqrt{\frac{A_{\mathrm{TW}}}{2}}\frac{(A_{\mathrm{TW}} + P_R^{\star})P_R^{\star}}{\sqrt{(2A_{\mathrm{TW}} - P_R^{\star})^3}}. \tag{14}$$

The upper bound on the power for error tolerance η can be evaluated numerically.

Fig. 1 depicts the tail ϵ for the TW channel. When $\Delta < 1$, the tail falls abruptly to zero at $P_R = A_{\mathrm{TW}}(1-\Delta)$. However, as it is seen from Fig. 1, the log-log slope that precedes this abrupt transition to zero is $\frac{1}{2}$ (half a decade per 10 dB), which can be also see from (13). In the singular case $\Delta = 1$ (0 dB), the tail approximation is given by (13) with $P_R^{\star} = P_R$ and the slope continues until $-\infty$ dB.[5] For example, if the log-log slope of $\frac{1}{2}$ should be present at $\epsilon = 10^{-6}$, then we need to have $\Delta > -4 \cdot 10^{-6}$dB, i.e. ρ_2 very close to ρ_1, which is unlikely in practice due to the losses of the reflected wave. Hence, the two-wave model should be used with high caution when evaluating URLLC scenarios.

B. Rayleigh Channel (Rayl)

This model, adopted in many wireless studies, has $\mu = 1$, $N = 0$ and $L = 1$ (single cluster and diffuse component and no specular components) and the envelope PDF is [12]:

$$f_{\mathrm{Rayl}}(r) = \frac{2r}{A_{\mathrm{Rayl}}}e^{-\frac{r^2}{A_{\mathrm{Rayl}}}}, \tag{15}$$

[5]The case $\Delta \approx 1$ has been referred to in the literature as hyper-Rayleigh fading [13]

with average power $A_{\mathrm{Rayl}} = 2\sigma^2$. The CDF follows readily as:

$$\epsilon = F_{\mathrm{Rayl}}(P_R) = 1 - e^{-\frac{P_R}{A_{\mathrm{Rayl}}}}, \tag{16}$$

which can be upper bounded by retaining only the first term in the Taylor expansion, resulting in the following simple power law approximation:

$$\tilde{\epsilon} = \frac{P_R}{A_{\mathrm{Rayl}}}, \tag{17}$$

also known as the Rayleigh rule of thumb "10dB outage margin per decade probability" due to a log-log slope of $\beta = 1$, see Fig. 1. The approximation error function can be derived via an upper bound on the Taylor remainder, yielding the simple form (see Appendix A):

$$\phi(P_R) = \frac{P_R}{2A_{\mathrm{Rayl}}}. \tag{18}$$

C. Rician Channel (Rice)

This is an extension of the Rayleigh channel, featuring a specular component in addition to the diffuse one. The average received power is $A_{\mathrm{Rice}} = \rho_1^2 + 2\sigma^2 = 2\sigma^2(k_1 + 1)$, where $k_1 = \frac{\rho_1^2}{2\sigma^2}$ is the Rician *k-factor* and the PDF of the received envelope is [12]:

$$f_{\mathrm{Rice}}(r) = f_{\mathrm{Rayl}}(r)e^{-k_1}I_0\left(\frac{r}{\sigma}\sqrt{2k_1}\right), \tag{19}$$

where $I_0(\cdot)$ is the modified Bessel function of 1st kind and 0th order. The tail can then be expressed in closed form in terms of the 1st order Marcum Q-function as follows:

$$\epsilon = F_{\mathrm{Rice}}(P_R) = 1 - Q_1\left(\sqrt{2k_1}, \sqrt{2\frac{P_R}{A_{\mathrm{Rice}}}(k_1+1)}\right). \tag{20}$$

Bounding ϵ from below via 1st polynomial expansion of Q_1, we arrive at the tail approximation:

$$\tilde{\epsilon} = \frac{P_R}{A_{\mathrm{Rice}}}(k_1+1)e^{-k_1}. \tag{21}$$

The approximation error function obtains the form (see Appendix A):

$$\phi(P_R) = e^{\frac{k_1}{2}}\left(e^{\frac{P_R}{A_{\mathrm{Rice}}}(k_1+1)} - 1\right), \tag{22}$$

The tail approximation of the Rician channel in UR-relevant regime has Rayleigh slope $\beta = 1$. However, Fig. 2 shows that before attaining the slope $\beta = 1$, the Rician CDF has a steeper slope compared to the Rayleigh one. In the context of wireless communications, this can be interpreted as an increased diversity order offered by the Ricean distribution. The lower the k_1-factor, the sooner the slope becomes identical to the Rayleigh one; in other words, as k_1 increases, P_R decreases for fixed error tolerance η which can be also see from (22).

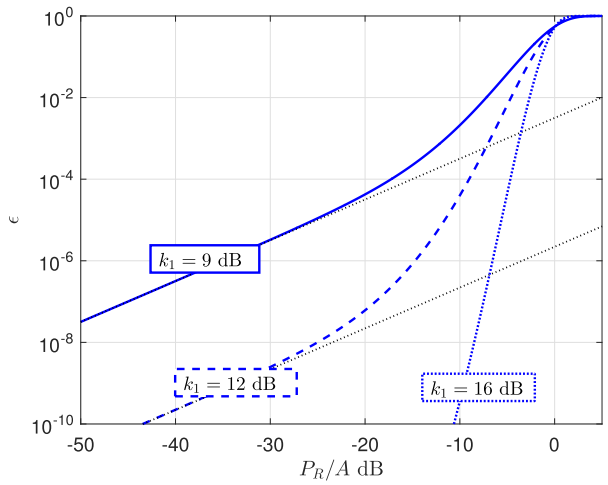

Fig. 2. Rician CDF (20) and its tail approximation (21) (black dotted lines): The Rician *k-factor* k_1 is indicated at the respective curves.

D. Weibull Channel (Wei)

The Weibull channel is a generalization of the Rayleigh model, where the diffuse component is given by $|V_{\text{dif}}| = \sqrt{(X_R^2 + X_I^2)^{1/\gamma}}$ with $\gamma \neq 1$ [15]. This model has been used in empirical studies to offer increased freedom to fit the modeling of the diffuse part. As in the Rayleigh case, here we also have only a diffuse component, but the received envelope follows Weibull distribution [15]:

$$f_{\text{Wei}}(r) = \frac{2\gamma r^{2\gamma-1}}{2\sigma^2} e^{-\frac{r^{2\gamma}}{2\sigma^2}}, \tag{23}$$

with $A_{\text{Wei}} = \left(2\sigma^2\right)^{1/\gamma} \Gamma(1+1/\gamma)$. For $\gamma = \frac{1}{2}$ we get the TW case, while $\gamma = 1$ leads to the Rayleigh case. The tail is given as:

$$\epsilon = F_{\text{Wei}}(P_R) = 1 - e^{-\left(\Gamma(1+1/\gamma)\frac{P_R}{A_{Wei}}\right)^{\gamma}}. \tag{24}$$

Using first order Taylor expansion, we obtain the following tail approximation:

$$\tilde{\epsilon} = \left(\Gamma(1+1/\gamma)\frac{P_R}{A_{\text{Wei}}}\right)^{\gamma}. \tag{25}$$

Here γ denotes the log-log slope β and an example with $\gamma = 2$ is shown in Fig. 3. The approximation error function for the Weibull channel is given by (see Appendix A):

$$\phi(P_R) = \frac{\left(\Gamma(1+1/\gamma)\frac{P_R}{A_{\text{Wei}}}\right)^{\gamma}}{1 + \left(\Gamma(1+1/\gamma)\frac{P_R}{A_{\text{Wei}}}\right)^{\gamma}}. \tag{26}$$

E. Nakagami-m Channel (Nak)

The envelope of this model behaves similarly to the Weibull model, although the diffuse component is modeled differently as $r = |V_{\text{dif}}| = \sqrt{\sum_{i=1}^{m}(X_{Ri}^2 + X_{Ii}^2)}$, with m integer. This model can be interpreted as an incoherent sum of m i.i.d. Rayleigh-type clusters, each with mean power $2\sigma^2$ and total power $A_{\text{Nak}} = m \cdot 2\sigma^2$. The PDF of the envelope r is given by [16]:

$$f_{\text{Nak}}(r) = \frac{2}{r\Gamma(m)} \left(\frac{r^2}{2\sigma^2}\right)^m e^{-\frac{r^2}{2\sigma^2}}, \tag{27}$$

where we interpret $m \in \mathbb{R} \geq \frac{1}{2}$ for generality. For $m = \frac{1}{2}$ we get an exponential, while for $m = 1$ a Rayleigh distribution. The CDF is given as:

$$\epsilon = F_{\text{Nak}}(P_R) = \frac{\gamma\left(m; m\frac{P_R}{A_{Nak}}\right)}{\Gamma(m)}, \tag{28}$$

where $\gamma(a, x)$ is the lower incomplete gamma function. The power law tail approximation can be obtained via the upper bound $\gamma(a; x) \leq x^a/a$ [17], resulting in:

$$\tilde{\epsilon} = \frac{m^m}{\Gamma(m+1)} \left(\frac{P_R}{A_{Nak}}\right)^m. \tag{29}$$

We see that (29) has the same flexibility and slope behavior as the Weibull model (for $m \geq \frac{1}{2}$), but a different offset. This can be also observed in Fig. 3 with $m = 2$, where the wide shoulder sends the tail (29) to lower levels compared with the Weibull case. By bounding the lower incomplete gamma function in (28) from both sides, i.e., $e^{-x}x^a/a \leq \gamma(a; x) \leq x^a/a$ [17], we derive the approximation error function:

$$\phi(P_R) = 1 - e^{-m\frac{P_R}{A_{\text{Nak}}}} \leq e^{m\frac{P_R}{A_{\text{Nak}}}} - 1. \tag{30}$$

F. $\kappa - \mu$ Channel ($\kappa\mu$)

The $\kappa - \mu$ model was developed in [18] as a generalization to the Nakagami model, by considering incoherent sum of μ Rician type clusters, i.e. envelope $r = \sqrt{\sum_{i=1}^{\mu}(X_{Ri} + p_i)^2 + (X_{Ii} + q_i)^2}$ where $X_{Ri} + jX_{Ii}$ are complex Gaussian diffuse components (all same mean power $2\sigma^2$) and $p_i + jq_i$ the corresponding specular components with arbitrary power $\rho_i^2 = p_i^2 + q_i^2$. Here κ is a generalized Rician type *k-factor* defined in (7). Consequently, the total mean power is $A_{\kappa\mu} = \mu(1+\kappa) \cdot 2\sigma^2$ and the PDF of r [18] is given by (31) (bottom of the next page). Again, for generality, we interpret $\mu \in \mathbb{R}$. The CDF in closed form is described via the generalized Marcum Q-function [18]:

$$\epsilon = F_{\kappa\mu}(P_R) = 1 - Q_\mu\left(\sqrt{2\kappa\mu}, \sqrt{2(1+\kappa)\mu P_R/A_{\kappa\mu}}\right). \tag{32}$$

Using a first-order polynomial expansion of the generalized Marcum Q-function, we obtain the following tail approximation:

$$\tilde{\epsilon} = \frac{(e^{-\kappa}(\kappa+1)\mu)^\mu}{\Gamma(\mu+1)} \left(\frac{P_R}{A_{\kappa\mu}}\right)^\mu, \tag{33}$$

i.e. a multiplicative form of the previous Rician and Nakagami-m tail approximation. The approximation error function obtains the simple form (see Appendix A):

$$\phi(P_R) = e^{\frac{\kappa\mu}{2}} \left(e^{(\kappa+1)\mu\frac{P_R}{A_{\kappa\mu}}} - 1\right). \tag{34}$$

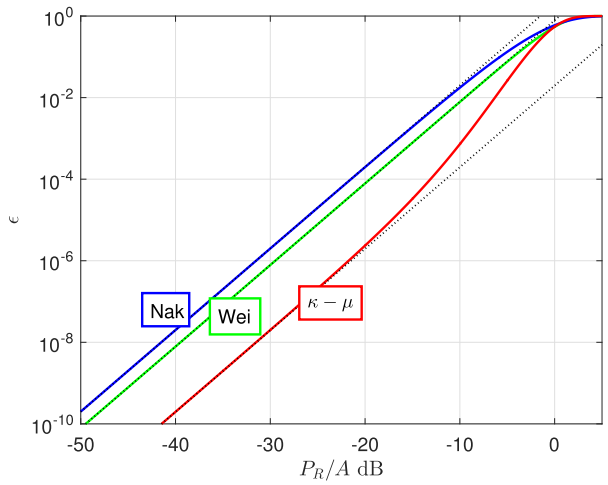

Fig. 3. Nakagami-m (28) ($m=2$), Weibull (24) ($\gamma=2$) and $\kappa-\mu$ (32) ($\kappa=3.9, \mu=2$) CDFs and their tail approximations (29),(25),(33) (black dotted lines).

We see that both $\tilde{\epsilon}$ and $\phi(P_R)$ reduce to the forms derived earlier as special cases; specifically, for $\mu=1$ the $\kappa-\mu$ model reduces to a Rician situation, while for $\kappa=0$ the Nakagami-m situation emerges.

The tail (33) in a typical Rician setting ($\kappa=3.9, \mu=2$) is seen in Fig. 3, where it can be seen that the tail is pushed to lower probabilities compared to Nakagami and Weibull models.

G. Generalizations

We analyze several generalizations of the channels presented in the previous subsection and derive their power law tail approximations. First, we explore the transition of the behavior from few paths to many paths. In this sense, we expand the previous TW model to cater for 3-vector components or include a diffuse part that is generalized compared to the models with diffuse part in the previous section. As it will be shown, both cases result in a tail behavior that conforms to a behavior dominated by diffuse components. In other words, three specular components can be sufficient to produce the behavior of a Rayleigh diffuse component at URLLC levels.

Another important generalization is to use combined short and long term processes, particularly when such are inseparable. We consider three combined models in following sub-sections: 1) Log-normal shadowed Rayleigh fading, i.e. the Suzuki distribution typically used to model Macro-cell behavior [12]; 2) $\kappa-\mu$ fading with Nakagami-m shadowing; and 3) $\kappa-\mu$ fading with inverse Gamma distributed shadowing. While 1) is a classical case, 2) and 3) have been found useful for modeling close range propagation [20], [21], [24].

We can think of the combined channel models to be applicable to the following situation. When there is only short term block fading, the outage probability can be controlled by selecting the rate R according to the known average power of the short term channel. Equally important is the specular component balancing or ratio towards the diffuse parts, captured by Δ, κ in (6), (7). However, when the sender does not have a reliable estimate of the average power (or impact of specular components), then this uncertainty can be modeled by assuming that the average power or Δ, κ are RVs. The independent sampling from the shadowing distribution is a pessimistic case that assumes sporadic transmissions, sufficiently separated in time.

1) Three-Wave Model (3W): We consider the Three-Wave generalization of the TW model. Here $N=3$, $V_{\rm dif}=0$, received envelope $r=|\rho_1+\rho_2 e^{j\phi_2}+\rho_3 e^{j\phi_3}|$ and average power $A_{\rm 3W}=\sum_{n=1}^{3}\rho_n^2$. The probability density function [7] is given by:

$$f_{\rm 3W}(r)=\begin{cases}\dfrac{\sqrt{r}}{\pi^2\sqrt{\rho_1\rho_2\rho_3}}K\left(\dfrac{\Delta_r^2}{\rho_1\rho_2\rho_3 r}\right) & \Delta_r^2\le\rho_1\rho_2\rho_3 r\\ \dfrac{r}{\pi^2\Delta_r}K\left(\dfrac{\rho_1\rho_2\rho_3 r}{\Delta_r^2}\right) & \Delta_r^2>\rho_1\rho_2\rho_3 r\end{cases} \tag{35}$$

for $r\in[r_{\min},r_{\max}]$, and it is 0 otherwise, with $r_{\min}=\max(2\max(\rho_1,\rho_2,\rho_3)-\rho_1-\rho_2-\rho_3,0)$, $r_{\max}=\rho_1+\rho_2+\rho_3$. In (35), $K(\cdot)$ is an elliptic integral of the first kind[6] and the quantity Δ_r is defined as:

$$\Delta_r^2=\frac{1}{16}[(r+\rho_1)^2-(\rho_2-\rho_3)^2][(\rho_2+\rho_3)^2-(r-\rho_1)^2]. \tag{36}$$

Without losing generality, we can take $\rho_1\ge\rho_2\ge\rho_3$ and define the difference $\Delta_\rho=\rho_1-(\rho_2+\rho_3)$, such that $r_{\min}=\max(\Delta_\rho,0)$. Three cases can be considered: (1) $r_{\min}=0$ when $\Delta_\rho<0$; (2) $r_{\min}=0$ and $\Delta_\rho=0$; and (3) $r_{\min}>0$ otherwise. Here we treat the case $\Delta_\rho<0$, which sets the basis for the reader to treat the other two cases. The integral (9) is evaluated for values $r\in[0,\sqrt{P_R}]$ that are very small and $\lim_{r\to0}\Delta_r^2=[\rho_1^2-(\rho_2-\rho_3)^2][(\rho_2+\rho_3)^2-\rho_1^2]>0$, which implies that $\Delta_r^2>\rho_1\rho_2\rho_3\, r$ holds in (35). With $r\to0$:

$$f_{\rm 3W}(r)\overset{r\to0}{\to}\frac{r}{\pi^2\Delta_r}K\left(\frac{\rho_1\rho_2\rho_3 r}{\Delta_r^2}\right)\approx\frac{r}{\pi^2\Delta_r}\frac{\pi}{2}, \tag{37}$$

where we have used $\lim_{x\to0}K(x)=\frac{\pi}{2}$. Approximating Δ_r^2 as a constant for small values of r, we get the following tail approximation:

$$\tilde{\epsilon}=\frac{r^2}{4\pi\Delta_r}=\frac{P_R}{4\pi\Delta_r}, \tag{38}$$

[6]Convention of [7] is $K(m)$ with argument $m=k^2$ (instead of $K(k)$ with modulus k).

$$f_{\kappa\mu}(r)=\frac{2(\kappa\mu)^{(1-\mu)/2}}{e^{\kappa\mu}\sqrt{2\sigma^2}}\left(\frac{r}{\sqrt{2\sigma^2}}\right)^{\mu}e^{\left(-\frac{r^2}{2\sigma^2}\right)}I_{\mu-1}\left[2\sqrt{\kappa\mu\frac{r^2}{2\sigma^2}}\right],\quad \mu\ge0. \tag{31}$$

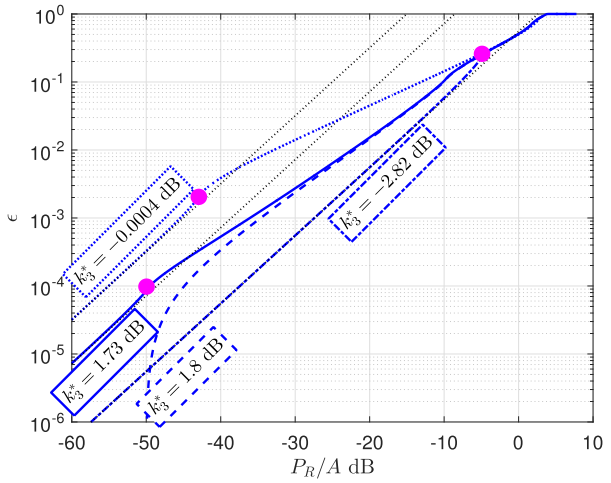

Fig. 4. Three Wave CDF (numerical integration of (35)) and the tail approximation (38) (black dotted line): Here $\rho_1 = 1$ while ρ_2 and ρ_3 are set according to k_3^* indicated at the curves. The solid dots depicts the locations of the "breaking points" where the asymptotic slopes change (as determined by the value of $|\Delta_\rho|^2$).

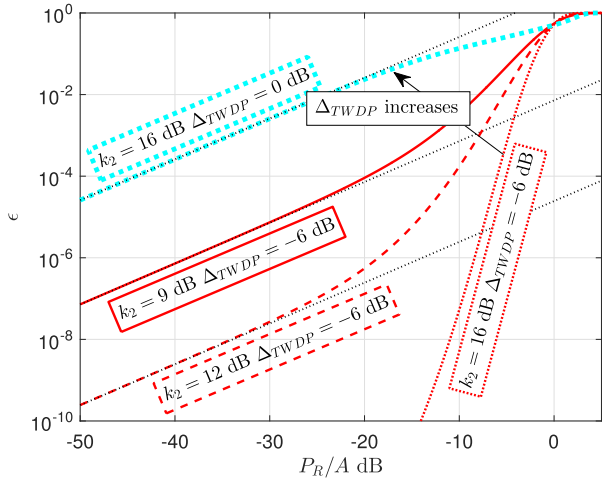

Fig. 5. Two-Wave Diffuse Power CDF and its tail approximation (black dotted line): $\rho_1 = 1$, while ρ_2 is set to correspond to the Δ (6) given at each curve. The corresponding k_2 (7) is also given.

such that the log-log linear slope is $\beta \approx 1$. In the singular case $r_{\min} = 0$ and $\Delta_\rho = 0$ it can be shown that $\beta = \frac{3}{4}$, while the case $r_{\min} > 0$ has a slope of $\frac{1}{2}, \frac{3}{4}$ or 1, before an abrupt fall to zero when $P_R = r_{\min}^2$.

The 3W CDF is shown in Fig. 4 for $\rho_1 = 1$ and different variations of ρ_2 and ρ_3. The curves are labeled by $k_3^* = \frac{\rho_1^2}{(\rho_2^2+\rho_3^2)}$.[7] We select to represent two cases with identical $10\log\frac{|\Delta_\rho|^2}{A_{3W}} = -50$dB that are seen to diverge significantly when $\frac{P_R}{A_{3W}} < -40$dB. The difference between these two cases emerges due to the different sign of Δ_ρ, which in one case results in $r_{\min} > 0$ ($\rho_2 = 0.7850$, $\rho_3 = 0.2109$) and in the other case $r_{\min} = 0$ ($\rho_2 = 0.7914$, $\rho_3 = 0.2126$). The latter case has a log-log slope of $\beta = 1$, identical to the Rayleigh distribution. Hence, if the sum of the two smallest components can cancel and overshoot the strongest component, the behavior of the 3W model is practically identical to that of a Rayleigh channel in terms of a slope in UR-relevant regime.

2) Two-Wave Diffuse Power (TWDP) Channel: In this model $N = 2$ and $V_{\rm dif}$, with envelope $r = |\rho_1 + \rho_2 + V_{\rm dif}|$ and average received power $A_{\rm TWDP} = \rho_1^2 + \rho_2^2 + 2\sigma^2$ [7]. The PDF is obtained by averaging of the Rician PDF [8]:

$$f_{\rm TWDP}(r) = \frac{1}{2\pi}\int_0^{2\pi} f_{\rm Rice}\left(r; k_2\left[1+\Delta\cos(\psi)\right]\right) d\psi, \tag{39}$$

with Δ defined in (6) and k_2 in (7). The integration over ψ involves only $I_0(\cdot)$ and the exponential terms in (19). Using $I_0 \geq 1$ for $\frac{P_R}{A_{\rm TWDP}} \ll \frac{1}{4k_2(k_2+1)}$, this integration is $\sim \frac{1}{2\pi}\int_0^{2\pi} e^{k_2\Delta\cos\psi}\cdot 1\, d\psi = I_0(k_2\Delta)$, i.e. it leads to a constant with respect to r. Hence, the tail can be lower-bounded through a scaled Rician tail:

$$\epsilon = F_{\rm TWDP}(P_R) \geq F_{\rm Rice}(P_R; k_2)\, I_0(k_2\Delta), \tag{40}$$

and the analysis from the Rician case can be directly applied, scaled by $I_0(k_2\Delta)$. From Fig. 5 it can be seen that TWDP[8] starts to differ from a Rician model (with $k_1 = k_2$) when Δ is sufficiently high, such that ρ_2 can be distinguished from $V_{\rm dif}$. The second specular component ρ_2 lifts-off the lower tail as $\Delta \to 0$ dB, while preserving the Rayleigh tail slope. Note that, in order to reach the extreme slope of the singular TW model at the URLLC levels, one needs $\Delta = 0$dB and k_2 in range 50 to 60dB, which is very unlikely to happen in practice.

3) Suzuki Channel (Suz): This is a compound channel consisting of a diffuse component only, which is a mixture between a Rayleigh envelope and a log-normal varying mean [12]. The compound envelope is $r = |X_R + jX_I|$, where X_R and X_I are zero-mean Gaussian variables with variance $\sigma_{\rm LN} = e^{\mathcal{N}}$ that has a log-normal distribution.

The PDF and CDF of the Suzuki channel can be found as follows. Let us denote by A the average power used to generate Rayleigh-faded power level A. The power A is log-normal distributed, such that we can obtain its PDF from the PDF of the log-normal envelope (53) by substituting $A = r^2$. This leads to the following joint distribution of P and A:

$$f_{\rm Suz}(P, A) = \frac{1}{A}e^{-\frac{P}{A}} \cdot \frac{1}{2A\sigma_l\sqrt{2\pi}} e^{-\frac{\left(\frac{1}{2}\ln A - \mu_l\right)^2}{2\sigma_l^2}}. \tag{41}$$

For given P_R, the tail can be calculated as follows:

$$\epsilon = F_{\rm Suz}(P_R) = \int_0^{P_R} {\rm d}P \int_0^{\infty} f_{\rm Suz}(P, A){\rm d}A. \tag{42}$$

[7]Note that this metric differs from the *k-factor* which involves diffuse parts. k_3^* is the ratio between specular component powers only

[8]No tractable closed form of PDF or CDF exists. In [7] the PDF is approximated, while we use a complete expansion as in [14]. However, due to the numerical sensitivity at URLLC levels, it requires the use of high-precision numerical tools.

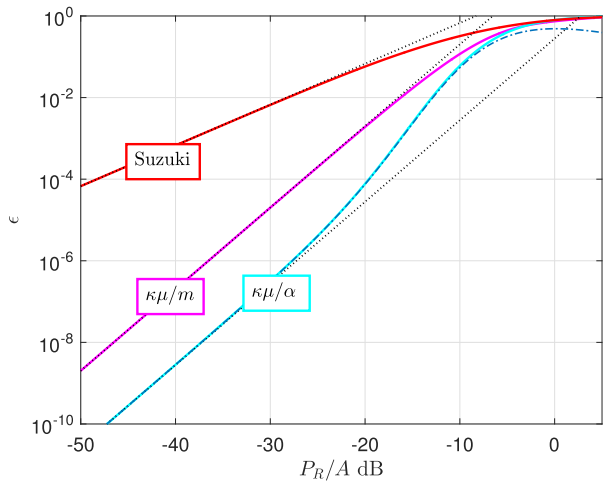

Fig. 6. Shadowed CDFs from (47) and numerical integration of (42),(49) and their tail approximations (45),(48),(51) (black dotted lines) and heuristic CDF expansion (52) (dash-dot curve): Suzuki ($\sigma_{dB} = 6$dB), $\kappa-\mu/m$ and $\kappa-\mu/\alpha$ ($\kappa = 3.9, \mu = 2, m = 0.25, \alpha = 1.5$).

The upper bound for (42) is obtained by noting that $\frac{P}{A} \geq 0$ and it can be removed from (41), after which we get:

$$\epsilon \leq \int_0^{P_R} \mathrm{d}P \int_0^{\infty} \frac{1}{2A^2\sigma_l\sqrt{2\pi}} e^{-\frac{\left(\frac{1}{2}\ln A-\mu_l\right)^2}{2\sigma_l^2}} \mathrm{d}A$$
$$= e^{2\sigma_l^2-2\mu_l} P_R = \frac{P_R}{A_{\mathrm{Suz}}} \cdot e^{4\sigma_l^2}, \tag{43}$$

where it can be found that $A_{\mathrm{Suz}} = e^{2\sigma_l^2+2\mu_l} = A_{\mathrm{LN}}$. The lower bound can be found by using the inequality $e^{-x} \geq 1-x$, resulting in

$$\epsilon \geq \frac{P_R}{A_{\mathrm{Suz}}} e^{4\sigma_l^2} - \left(\frac{P_R}{A_{\mathrm{Suz}}}\right)^2 \cdot e^{12\sigma_l^2} \tag{44}$$
$$\approx \frac{P_R}{A_{\mathrm{Suz}}} e^{4\sigma_{\mathrm{dB}}^2 \frac{\ln(10)^2}{20^2}} = \tilde{\epsilon}. \tag{45}$$

For UR-relevant levels it is $P_R \ll A_{\mathrm{Suz}}$, such that the upper bound can be treated as tight. The tail has a Rayleigh-like slope of $\beta = 1$, but pushed to lower levels as seen in Fig. 6.

4) Nakagami-m Shadowed $\kappa-\mu$ Channel ($\kappa\mu/m$): Shadowing the total signal has been investigated in [20] and [21], but provides complicated PDF and no known closed-form solution for the CDF. A model that considers shadowing of only the dominant signal parts has been developed by [24]. The instant power is $p = \sum_{i=1}^{\mu}(X_{Ri}+\xi p_i)^2 + (X_{Ii}+\xi q_i)^2$, where ξ is a power normalized Nakagami-m distributed shadowing amplitude acting on specular components $p_i + jq_i = \rho_i e^{j\phi_i}$. The closed form PDF of P_R [24] (with $p = P_R/A_{\kappa\mu/\mathrm{m}}$) is given by (46) (top of the next page) with ${}_1F_1(\cdot)$ denoting Kummer's function of the first kind [34]. Essentially, the first part is a Nakagami-m PDF of order μ, while the latter part holds a $\mu-$order modified Rician impact. The tail is given by (47) (also at the top of the next page) where $\Phi_2(\cdot)$ is Humberts function [25] with arguments $(b_1 = \mu-m, b_2 = m, c = \mu+1, x = -\mu(1+\kappa)\frac{P_R}{A_{\kappa\mu/\mathrm{m}}}, y = x\frac{m}{\kappa\mu+m})$. The power law tail approximation is

$$\tilde{\epsilon} = \frac{\mu^\mu(\kappa+1)^\mu}{\Gamma(\mu+1)} \left(\frac{P_R}{A_{\kappa\mu/\mathrm{m}}}\right)^\mu \left(\frac{m}{\kappa\mu+m}\right)^m, \tag{48}$$

following from [24, eq. (13)]. Since $\xi \to 1$ when $m \to \infty$, expression (47) should reduce to the regular $\kappa-\mu$ in (33); this is indeed so, as $\left(\frac{x+m}{m}\right)^m \to e^x$ and (47) is in accordance with (33). Fig. 6 shows a strongly shadowed example ($m = 0.25$). It can be noticed that the shoulder is significantly broadened to a degree that the elevation of the shoulder visible in the regular $\kappa-\mu$ case, has vanished. This is expected as only the LOS part has been shadowed, thereby effectively averaging the $\kappa-\mu$ distributions shape (κ-factor). Consequently, the tail is being pushed to significantly lower outages.

5) Inverse $\Gamma-$Shadowed $\kappa-\mu$ Channel ($\kappa\mu/\alpha$): Shadowing the total $\kappa-\mu$ (31) fading envelope $r_{\kappa\mu} = |V_{\kappa\mu}|$ by an inverse Gamma (Γ^{-1}) distributed varying mean power $\omega = A_{\kappa\mu}$, leads to a closed form PDF but no tractable closed-form CDF solution [21].[9] The combined signal ($r = r_{\kappa\mu}\sqrt{\omega}$) PDF is obtained [21, eq. (6)] by averaging the conditional envelope PDF $f_{\kappa\mu|A_{\kappa\mu}}$ (31) over the mean power statistics $f_{\Gamma^{-1}}(\omega) = \frac{\beta^\alpha}{\Gamma(\alpha)}\frac{1}{\omega^{\alpha+1}} \cdot \exp\left(-\frac{\beta}{\omega}\right)$, with shape $\alpha > 0$ and scale $\beta > 0$ parameters. The combined signal power PDF of [21, eq. (10)] can be written as in (49) (top of the next page) with $B(\cdot,\cdot)$ denoting the beta function and argument scaling $c = \frac{\mu(1+\kappa)}{\beta}$ in $x = \kappa\mu\frac{c\cdot p}{c\cdot p+1}$. The relative power is $p = \frac{r^2}{E[r^2]} = \frac{P_R}{A_{\kappa\mu/\alpha\beta}}$ and $A_{\kappa\mu/\alpha\beta}$ is the mean power of the combined signal. For lower tail levels $p \ll \frac{1}{c}$ or $\alpha \to 1^+$, $(c\cdot p+1)^{\alpha-1} \to 1$ and constraining this approximation to the leading term only, we essentially have a function of form $f(x) = x^{b-1}{}_1F_1(a,b,x)$. To obtain the CDF we make use of $\int f(x)dx = x^b\frac{\Gamma(b)}{\Gamma(b+1)}{}_1F_1(a,b+1,x)$ [23]. Thus, via variable transform and reordering of terms, we arrive at the upper bound (50) (top of the next page) for the CDF; the upper bound is tight in the limit $\alpha \to 1^+$. Furthermore, we can simplify (50) as ${}_1F_1(a,b,x) \to 1$ for $x \to 0$ and realizing that the scale β in [21] is set arbitrarily, such that $f_{\Gamma^{-1}}$ is not normalized. As $\overline{\omega} = E[\omega] = \frac{\beta}{\alpha-1}$ valid for $\alpha > 1$ [21], normalizing shadowing by setting $\overline{\omega} = 1$, we get $\beta = \alpha-1$. Thus, we can represent the impact of the shadowing through a single parameter:

$$F_{\kappa\mu/\alpha}(P_R) \gtrsim \underbrace{\frac{(\mu(1+\kappa)e^{-k})^\mu}{\Gamma(1+\mu)} p^\mu}_{\approx F_{\kappa\mu}(p;\kappa;\mu)} \frac{\Gamma(\alpha+\mu)}{(\alpha-1)^\mu\Gamma(\alpha)}, \tag{51}$$

i.e. in form of a scaled $\kappa-\mu$ tail, representing a lower bound; for $\alpha \lesssim 1$ other normalization methods must be used.

We can heuristically reintroduce the denominator term $(c\cdot p+1)^{\alpha-1}$ into the leading term of (50) for larger arguments, leading to the lower bound (52) (top of the next page) where

[9] Very recently [22, eq. (3.14)] has provided a closed-form CDF. However, this is provided through a complex Kampé de Fériet function, for which no readily available numerical evaluation exists in tools such as Matlab$^{\mathrm{TM}}$. Furthermore, no simple analytical approximation seems available to be used in an URC setting. The underlying inverse Gamma PDF in [22, eq. (3.14)] seems normalized in a skewed manner with $\overline{\omega} = \frac{\alpha}{\alpha-1}$. Thus we make our approximation analysis based on the PDF in [21].

$$f_{\kappa\mu/\mathrm{m}}(P_R) = \frac{\mu^\mu}{\Gamma(\mu)A_{\kappa\mu/\mathrm{m}}} p^{\mu-1} e^{-(1+\kappa)\mu\cdot p} \left(\frac{m}{\kappa\mu+m}\right)^m {}_1F_1\left(m;\mu;\frac{\kappa(1+\kappa)\mu^2}{\kappa\mu+m}p\right). \tag{46}$$

$$\epsilon = F_{\kappa\mu/\mathrm{m}}(P_R) = \underbrace{\frac{\mu^\mu}{\Gamma(\mu+1)}\left(\frac{P_R}{A_{\kappa\mu/\mathrm{m}}}\right)^\mu}_{\approx F_{Nak}(p;\mu)} (\kappa+1)^\mu \underbrace{\left(\frac{m}{\kappa\mu+m}\right)^m}_{\to e^{-\kappa\mu}|m\to\infty} \Phi_2(b_1,b_2;c,x,y). \tag{47}$$

$$f_{\kappa\mu/\alpha\beta}(P_R) = \frac{(e^{-k}/\kappa\mu)^\mu}{B(\alpha,\mu)\,(c\cdot p+1)^{\alpha-1}} \cdot \frac{\kappa\mu\cdot c/A_{\kappa\mu/\alpha\beta}}{(c\cdot p+1)^2} x^{\mu-1} {}_1F_1\,(\alpha+\mu;\mu;x). \tag{49}$$

$$\epsilon = F_{\kappa\mu/\alpha\beta}(P_R) \le \frac{e^{-\kappa\mu}}{\mu B(\alpha,\mu)}\left(\frac{c\cdot p}{c\cdot p+1}\right)^\mu \cdot {}_1F_1\left(\alpha+\mu;\mu+1;\kappa\mu\frac{c\cdot p}{c\cdot p+1}\right). \tag{50}$$

$$\epsilon = F_{\kappa\mu/\alpha}(P_R) \gtrsim \frac{e^{-\kappa\mu}}{\mu B(\alpha,\mu)(c\cdot p+1)^{\alpha-1}}\left(\frac{c\cdot p}{c\cdot p+1}\right)^\mu \cdot {}_1F_1\left(\alpha+\mu;\mu+1;\kappa\mu\frac{c\cdot p}{c\cdot p+1}\right). \tag{52}$$

we can redefine $c = \frac{\mu(1+\kappa)}{\alpha-1}$ via the above normalization. This result provides a significantly better fit than (50) or (51), especially in a strongly shadowed Rician regime ($\kappa/\alpha \gtrsim 1$), as it can be seen in Fig. 6. It is also seen that the elevated shoulder from the underlying $\kappa-\mu$ signal is better preserved than in the case of the previous $\kappa\mu/m$ model, while also having strong shadowing ($\alpha = 1.5$) that indicates that the complete signal has been shadowed.

IV. Other Channels

In this section we analyze two special models that do not exhibit power-law tail behavior and derive their corresponding tail approximations. First, we consider the log-normal distribution [12], as a classical reference distribution for shadowing. Next, we treat cascaded type of channel models that arise in NLOS propagation, backscatter communication and in 'pin hole' channels [12]. The two models also represent two extremes, the macro scale (log-normal shadowing) and short range (e.g. device-to-device). Furthermore, these models can be used to illustrate cases that do not follow the power law in the diversity analysis presented in the next section.

A. Log-Normal Channel (LN)

In this model there is a single specular component $N = 1$ and no diffuse component. The specular component is not constant, but subject to a log-normal shadowing, such that log-envelope $\ln(r)$ has the following PDF [12]:

$$f_{\mathrm{LN}}(r) = \frac{1}{r}\mathcal{N}_{\ln(r)}(\mu_l,\sigma_l) = \frac{1}{r\sigma_l\sqrt{2\pi}} e^{-\frac{(\ln(r)-\mu_l)^2}{2\sigma_l^2}}, \tag{53}$$

with logarithmic mean $\mu_l = E[\ln(r)] = \mu_{\mathrm{dB}}\frac{\ln(10)}{20}$ and standard deviation $\sigma_l = \sqrt{E[\ln(r)^2]-\mu_l^2} = \sigma_{\mathrm{dB}}\frac{\ln(10)}{20}$. The average power is $A_{\mathrm{LN}} = e^{2\sigma_l^2+2\mu_l}$ [12] and the CDF is

$$\epsilon = F_{\mathrm{LN}}(r) = \tfrac{1}{2} + \tfrac{1}{2}\mathrm{erf}(x(r)), \tag{54}$$

with $x = (\ln(r)-\mu_l)/(\sigma_l\sqrt{2})$ and erf denoting the error function. Using Bürmann-type asymptotic approximation [28] leads to $F_{\mathrm{LN}}(x) \approx \frac{1}{2}\left(1+\mathrm{sgn}(x)\sqrt{1-e^{-x^2}}\right) \approx \frac{1}{4}e^{-x^2}$, when omitting higher order terms and approximating the square root for $|x| \gg 0$. A tighter approximation can be obtained if we use $F_{\mathrm{LN}}(x) \approx \frac{1}{4}e^{-f(x)}$ with a polynomial fitting function $f(x)$ [29]. Comparing $\frac{1}{4}e^{-x^2}$ with (54), it appears to be shifted proportionally to σ_l, such that

$$\epsilon = F_{\mathrm{LN}}(P_R) \approx \tfrac{1}{4}e^{-\frac{\left(\frac{1}{2}\ln(P_R)-a\sigma_l-\mu_l\right)^2}{2\sigma_l^2}} = \tilde{\epsilon}. \tag{55}$$

With $a = 0.223$, the relative error is $\eta \lesssim 10^{-1}$ for $10^{-12} \le \epsilon \le 10^{-2}$ and $3 \le \sigma_{\mathrm{dB}} \le 24$dB. The deviation on the margin matters most for outage analysis and here is below $\frac{1}{3}$dB. This accuracy is still very useful, considering the simplicity of the expression for analytical studies. Solving (55) for P_R and fixed $\tilde{\epsilon}$, we get

$$P_R \approx e^{2[(a\sigma_l+\mu_l)+\sqrt{2}\sigma_l\sqrt{-\ln(\tilde{\epsilon})+\ln(1/4)}]}. \tag{56}$$

For a given P_R, we can find the log-log slope as $\beta = \frac{d\log(\tilde{\epsilon})}{d\log(P_R)} \approx \frac{10}{\ln 10}\left[\frac{a}{\sigma_{\mathrm{dB}}} - 2\frac{P_{R,\mathrm{dB}}-\mu_{\mathrm{dB}}}{2\sigma_{\mathrm{dB}}^2}\right]$. From Fig. 7 it is observed that, for large σ_{dB}, a log-normal channel can exhibit extreme slopes when the level $\frac{P_R}{A}$ is in the region -10 to -30 dB, which makes it hard to distinguish from a TW or TWDP channel. However, when going towards UR-relevant levels, the deviation from a linear slope is noticeable.

B. Cascaded Rayleigh Channel (Cas)

This model also contains only a diffuse component, which is a product of the envelopes of two Rayleigh links r_1 and r_2. The compound received envelope is $r = r_1r_2 = |X_{R_1} + jX_{I_1}|\cdot|X_{R_2}+jX_{I_2}|$ with PDF equal to [26], [27]

$$f_{\mathrm{Cas}}(r) = \frac{r_\Gamma}{\sigma_1\sigma_2} I_0\left(r_\Gamma\sqrt{\Gamma}\right) K_0\left(r_\Gamma\right), \tag{57}$$

where $r_\Gamma = \frac{r}{\sigma_1\sigma_2(1-\Gamma)}$. Using (57) we get $A_{\mathrm{Cas}} = E[r^2] = 4\sigma_1^2\sigma_2^2(1+\Gamma) = P_1P_2(1+\Gamma)$ with correlation coefficient Γ between powers $P_1 = r_1^2$ and $P_2 = r_2^2$. I_n and K_n are the

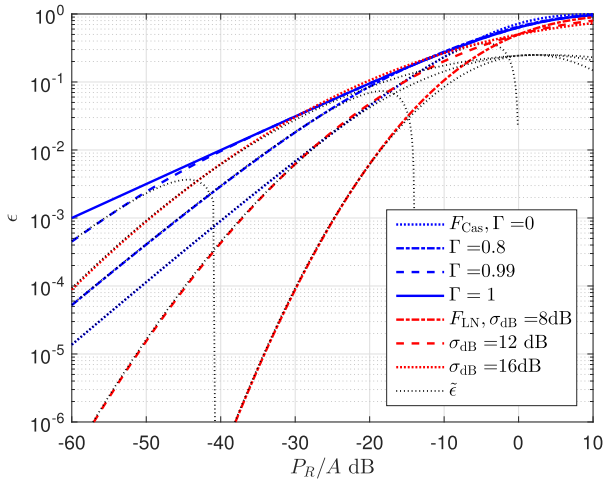

Fig. 7. Cascaded Rayleigh (58) with equal power links ($\sigma_1 = \sigma_2 = \sigma$) - and Log-Normal (54) distributions, for different values of the parameters. Dotted curves: tail approx. (59), (55).

Modified Bessel functions of 1st and 2nd kind, of order n. The CDF follows as:

$$\begin{aligned}\epsilon &= F_{\text{Cas}}(r) \\ &= 1 - r_\Gamma \left[\sqrt{\Gamma} I_1\left(r_\Gamma \sqrt{\Gamma}\right) K_0\left(r_\Gamma\right) + I_0\left(r_\Gamma \sqrt{\Gamma}\right) K_1\left(r_\Gamma\right)\right].\end{aligned} \tag{58}$$

Approximating the Bessel functions for $r_\Gamma \ll 1$, the general case ($\Gamma < 1$) simplifies as

$$\epsilon = F_{\text{Cas}}(P_R) \approx -\frac{P_R}{A_{\text{Cas}}} \frac{1+\Gamma}{1-\Gamma} \ln\left(\frac{P_R}{A_{\text{Cas}}} \frac{1+\Gamma}{(1-\Gamma)^2}\right) = \tilde{\epsilon}, \tag{59}$$

where γ is Euler's constant. The slope is found as $\beta \approx \frac{d\log(\tilde{\epsilon})}{d\log\frac{P_R}{A_{\text{Cas}}}}$, leading to $\beta \approx 1 + \frac{1}{\ln\left(\frac{P_R}{A_{\text{Cas}}}\right) + \ln\frac{1+\Gamma}{(1-\Gamma)^2}}$ and it gradually approaches a Rayleigh slope for $\frac{P_R}{A_{\text{Cas}}} \to 0$. For $\Gamma = 0$ the model collapses to the double-Rayleigh model [11].

For the singular case of $\Gamma = 1$ ($r_1 = r_2$), simple deduction yields $r_{\text{Cas}} = r_1 r_2 = F^{-1}_{\text{Cas}}(\epsilon) = F^{-1}_{\text{Rayl}}(\epsilon)^2 = r^2_{\text{Rayl}}$. Thus, $F_{\text{Cas}}(P_R) = F_{\text{Rayl}}(\sqrt{P_R}) \sim \sqrt{\frac{P_R}{A_{\text{Rayl}}}}$ and the slope $\beta \approx \frac{1}{2}$ is identical to the singular case of a TW model. It can be concluded from Fig. 7 that a the log-log behavior of cascaded Rayleigh fading can be represented by two different slopes with a breakpoint.

V. Simplified Analysis of Diversity Schemes

In practice, attaining very high reliability levels with reasonable power can only happen by having high levels of diversity at the receiver. Our analysis has shown that the tail approximation at the URC levels mostly has the form given in (1), which can be used for simplified diversity analysis in cases in which the full PDF and/or CDF are not tractable. For small terminals, the main impairment towards exploiting multi-antenna, i.e., multi-branch diversity is the branch power ratio (BPR), which for the pair of the $m-$th and $n-$th antenna is defined as $\text{BPR}_{\text{mn}} = \frac{A_m}{A_n}$ [30], [31]. In the following we assume that the receiver has M antennas that are not correlated, i.e., the received signals across antennas are independent non-identically distributed (i.n.i.d.) RVs.

In Selection Combining (SC), only the strongest signal among the M antennas is selected:

$$P_{R,\text{SC}} = \max(P_1, .., P_M). \tag{60}$$

For independent branches, the CDF can be expressed as a simple product of the individual CDFs across branches:

$$\epsilon = F_{\text{SC}}\left(P_R\right) = \prod_{m=1}^{M} F_m\left(P_R\right). \tag{61}$$

When Maximum Ratio Combining (MRC) is used, the received power is:

$$P_{R,\text{MRC}} = \sum_{m=1}^{M} P_m. \tag{62}$$

We derive an approximation of the CDF for general M-branch MRC (see Appendix B):

$$\epsilon = F_{\text{MRC}}(P_R) \approx \underbrace{\frac{\prod_{m=1}^{M}\Gamma(1+\beta_m)}{\Gamma(1+\sum_{m=1}^{M}\beta_m)}}_{\alpha_{\text{MRC}}} \underbrace{\prod_{m=1}^{M} \alpha_m \left(\frac{P_R}{A_m}\right)^{\beta_m}}_{\sim F_{SC} = \prod F_m} = \tilde{\epsilon}. \tag{63}$$

Note that this solution also splits into an MRC weighting term α_{MRC}, which depends solely on the branch slopes β and correctly collapsing to 1 for $M = 1$, and a term similar to SC $F_{\text{SC}} = \prod F_m$, which involves the offsets α_m. The distribution specific parameters α_m, β_m for this simple expression, are given in Table I. Inserting $\alpha_{\kappa\mu/m}$ and $\beta_{\kappa\mu/m}$ from Table I, does indeed produce the distribution specific MRC solution for shadowed $\kappa - \mu$ fading given in [24, eq. (18)]. When all branch slopes are equal $\beta_m = \beta$, we get:

$$\epsilon = F_{\text{MRC}}(P_R) \approx \underbrace{\frac{\Gamma(1+\beta)^M}{\Gamma(1+\beta M)}}_{\alpha_{\text{MRC}}} \underbrace{\left(\frac{P_R}{A_1}\right)^{\beta M} \prod_{m=1}^{M} \frac{\alpha_m}{\text{BPR}_m^{\beta}}}_{\sim F_{SC} = \prod F_m} = \tilde{\epsilon} \tag{64}$$

with $\text{BPR}_m = A_m/A_1$. A heuristic simplification is $\alpha_{\text{MRC}} \sim \frac{1}{M!^{\beta}}$, with outage error $\lesssim$ 1dB for $M = 4$ and $\lesssim$ 1.5dB for $M = 8$, both at 10^{-6} probability and for $\frac{1}{2} \lesssim \beta \lesssim 2$.

Using (63), we can bound the tail approximation error using the approximation error functions derived previously, yielding:

$$\phi_{\text{MRC}}(P_R) = (1 + \phi^{\max}(P_R))^M - 1, \tag{65}$$

with $\phi^{\max}(P_R) = \max(\phi_1(P_R), \ldots, \phi_M(P_R))$. Using Bernoulli approximation, we arrive at the intuitive expression $\phi_{\text{MRC}}(P_R) \approx M\phi^{\max}(P_R)$, which can be used for quick evaluation of the upper bound on the power P_R for given error tolerance η.

Finally, based on (63) it is easy to make a heuristic generic expansion by considering local log-log linear approximation of *any* CDF tail. This is e.g. the case for Log-Normal and

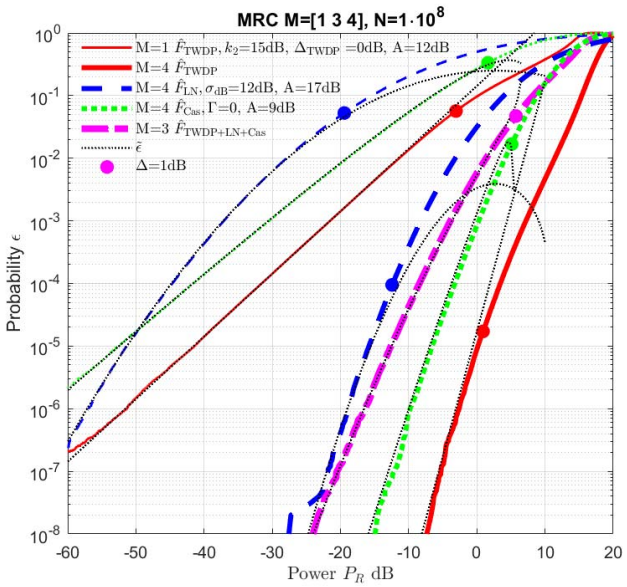

Fig. 8. MRC with $M = 4$ for i.i.d. TWDP, Log-Normal and Double-Rayleigh (Cascaded Rayleigh with $\Gamma = 0$). Also MRC with $M = 3$ for one branch of each of the distributions. Bolder curves are obtained by simulation, thin dotted lines are the tail approximations. (40), (59), (55) and MRC (66), (63). Bold dots represent 1dB deviation of tail vs. simulation.

Cascaded Rayleigh models,[10] where the branch slopes depend on the power levels $\beta(P_R/A)$:

$$\epsilon = F_{\rm MRC}(P_R) \approx \alpha_{\rm MRC}(\beta_1(P_R)..\beta_M(P_R))F_{\rm SC}\left(P_R\right) = \tilde{\epsilon}, \tag{66}$$

with $\alpha_{\rm MRC}$ given in (63) or simplified in (64) when all branches have the same slope. With this structure and availability of slopes $\beta(P_R)$, one can use the full CDFs in F_{SC}.

Fig. 8 shows Monte Carlo simulation with 10^8 samples of TWDP, Log-Normal and Double-Rayleigh (Cascaded Rayleigh with $\Gamma = 0$) distributions with different mean powers. Each distribution is further circularly shifted to provide uncorrelated copies for i.i.d. $M = 4$. It is observed how the single branch tail approximations (thin lines) follow the simulations up to the onset of the shoulders. The $4-$branch MRC tail approximation shows very good fit at URLLC probabilities - bold dots indicate point of 1dB deviation to the simulation. Furthermore, from the log-normal and 3-branch cross-distribution MRC, it is observed that the heuristic expansion in (66) indeed provides very useful results.

VI. Discussion and Conclusions

We have investigated the properties of wireless channel models in the URC regime and developed approximations of the tail distributions. Our analysis has shown that, for a wide range of practical models, the outage probability at URC levels depends on the minimal required decoding power through an exponent β which, for the case of Rayleigh fading is $\beta \approx 1$. More importantly, it has also been shown that the outage probability also depends on a tail offset α, which is strongly dependent on specific specular and diffuse part combinations. The previous URC studies [32] have resorted to Rayleigh models, without an argumentation for the usefulness at UR-relevant levels. Our analysis reveals that the main factor affecting the tail probability is the tail offset α, rather than the exponent β of the derived power law outage model. Furthermore, the power law tail descriptions provides an 'umbrella' model structure, circumventing the need for any prior decision on a specific model. This feature is particularly useful when no empirical studies are available to suggest which model to use. Hence, when conducting empirical studies that work with these models, one should account for the large uncertainty that occurs when assessing the models at the URC levels and collect proportionally large number of samples. Finally, we have provided a simplified analysis of MRC diversity for power-law tails, as well as a heuristic expansion. This paves the way for more elaborate diversity analysis, which is vital for achieving ultra-reliable operation with reasonable data rates.

[10]or some of the more elaborate tails, like for $\kappa - \mu$ type models.

Appendix A
Derivation of the Approximation Error Function

A. Two-Wave Model

We derive the tail for the general case when $\Delta \leq 1$ (which includes $\Delta = 1$ as a special case). By definition the tail is the solution to the following integral:

$$\epsilon = \int_{\sqrt{A_{\rm TW}(1-\Delta)}}^{\sqrt{P_R}} \frac{2r}{\pi A_{\rm TW}\sqrt{\Delta^2 - \left(1 - \frac{r^2}{A_{\rm TW}}\right)^2}} dr. \tag{67}$$

We introduce the following variable $x \equiv x(r) = \sqrt{\frac{1}{\Delta}r^2 - \frac{1-\Delta}{\Delta}A_{\rm TW}}$: Using change of variables, the integral (67) can be written as follows:

$$\epsilon = \int_0^{\sqrt{P_R^\star}} \frac{2x}{\pi A_{\rm TW}\sqrt{1 - \left(1 - \frac{x^2}{A_{\rm TW}}\right)^2}} dx, \tag{68}$$

where $P_R^\star = x^2(P_R)$. Even though the CDF has a closed form expression, bounding the sum of the higher order terms of its series expansion is difficult. We use an alternative approach instead. Specifically, we expand the integrand into Taylor series in the interval $[0, x), x \geq 0, x \to 0$ using Lagrange form for the remainder (i.e., the sum of the remaining higher order terms):

$$f(x) = f(0) + \frac{f'(0)}{1!}x + \frac{f''(\delta)}{2!}x^2, \tag{69}$$

for $\delta \in (0, x)$. Then, we bound the remainder from above, relying on the fact that integrating will not change the inequality;

we obtain the following:

$$\epsilon = \int_0^{\sqrt{P_R^\star}} \left(\frac{1}{\pi}\sqrt{\frac{2}{A_{\mathrm{TW}}}} + \frac{4(A_{\mathrm{TW}}-\delta^2)}{\pi\sqrt{(2A_{\mathrm{TW}}-\delta^2)^3}}x^2 \right) dx \quad (70)$$

$$\leq \int_0^{\sqrt{P_R^\star}} \left(\frac{1}{\pi}\sqrt{\frac{2}{A_{\mathrm{TW}}}} + \frac{4(A_{\mathrm{TW}}-P_R^\star)}{\pi\sqrt{(2A_{\mathrm{TW}}-P_R^\star)^3}}x^2 \right) dx \quad (71)$$

$$= \frac{1}{\pi}\sqrt{\frac{2}{A_{\mathrm{TW}}}}\sqrt{P_R^\star}\left(1 + \frac{4}{3}\sqrt{\frac{A_{\mathrm{TW}}}{2}}\frac{(A_{\mathrm{TW}}-P_R^\star)P_R^\star}{\pi\sqrt{(2A_{\mathrm{TW}}-P_R^\star)^3}}\right), \quad (72)$$

Recognizing that (72) can be written as $\epsilon \leq \tilde{\epsilon}(1+\phi(P_R))$, we extract $\phi(P_R)$ as the second term in the brackets in (72), completing the derivation. Note that in (71) we used the fact that the multiplicative term in front of x^2 increases monotonically with $\delta \in (0, x)$; hence we bound it from above with $x = \sqrt{P_R^\star}$.

B. Rayleigh Model

Deriving the approximation error function follows similar steps as in the TW case, except that we directly bound the Lagrange remainder of the Taylor series expansion of the tail in the interval $[0, P_R), P_R \to 0$. Hence, we obtain:

$$\epsilon \geq \frac{P_R}{A_{\mathsf{Rayl}}} - \frac{P_R^2}{2A_{\mathsf{Rayl}}^2} = \frac{P_R}{A_{\mathsf{Rayl}}}\left(1 - \frac{P_R}{2A_{\mathsf{Rayl}}}\right), \quad (73)$$

which completes the derivation.

C. Weibull Model

We use the inversion:

$$P_R = \frac{A_{\mathrm{Wei}}}{\Gamma(1+1/\gamma)}\left(-\ln(1-\epsilon)\right)^{\frac{1}{\gamma}}, \quad (74)$$

and the following bounds:

$$\epsilon + \frac{\epsilon^2}{(1-\epsilon)} \geq -\ln(1-\epsilon) \geq \epsilon. \quad (75)$$

The upper bound in (75) has been derived by bounding from above the remainder of the Taylor expansion of the function $-\ln(1-\epsilon)$ in the interval $[0, \epsilon)$, i.e.:

$$\frac{\epsilon^2}{2(1-\epsilon)^2} \leq \frac{\epsilon^2}{(1-\epsilon)}, \quad (76)$$

for $\epsilon \geq 0$. Replacing (75) into (74) and inverting for ϵ, we get:

$$\tilde{\epsilon} \geq \epsilon \geq \tilde{\epsilon}\frac{1}{1+\left(\Gamma(1+1/\gamma)\frac{P_R}{A_{\mathsf{Wei}}}\right)^\gamma} \quad (77)$$

$$= \tilde{\epsilon}\left(1 - \frac{\left(\Gamma(1+1/\gamma)\frac{P_R}{A_{\mathsf{Wei}}}\right)^\gamma}{1+\left(\Gamma(1+1/\gamma)\frac{P_R}{A_{\mathsf{Wei}}}\right)^\gamma}\right), \quad (78)$$

completing the drivation.

D. Rician, Nakagami-m and $\kappa-\mu$ Model

We derive the approximation error function only for the general $\kappa-\mu$ model; the corresponding error functions for the Rician and Nakagami-m models can be obtained as special cases.[11] We use polynomial series expansion for the generalized Marcum Q-function via generalized Laguerre polynomials and write the CDF as follows [19]:

$$\epsilon = e^{-\kappa\mu}\sum_{n=0}^{\infty}(-1)^n\frac{L_n^{(\mu-1)}(\kappa\mu)}{\Gamma(\mu+n+1)}\left((\kappa+1)\mu\frac{P_R}{A_{\kappa\mu}}\right)^{n+\mu}, \quad (79)$$

where $L_n^{(\alpha)}(\cdot)$ is the generalized Laguerre polynomial of degree n and order α. Recognizing that the first term in the above sum gives the power law approximation $\tilde{\epsilon}$, we obtain the following:

$$|\epsilon-\tilde{\epsilon}| = \left| e^{-\kappa\mu}\sum_{n=1}^{\infty}(-1)^n\frac{L_n^{(\mu-1)}(\kappa\mu)}{\Gamma(\mu+n+1)}\left((\kappa+1)\mu\frac{P_R}{A_{\kappa\mu}}\right)^{n+\mu}\right| \quad (80)$$

$$\leq e^{-\kappa\mu}\sum_{n=1}^{\infty}\frac{|L_n^{(\mu-1)}(\kappa\mu)|}{\Gamma(\mu+n+1)}\left((\kappa+1)\mu\frac{P_R}{A_{\kappa\mu}}\right)^{n+\mu} \quad (81)$$

$$\leq \frac{e^{-\frac{\kappa\mu}{2}}}{\Gamma(\mu)}\sum_{n=1}^{\infty}\frac{\Gamma(\mu+n)}{n!\Gamma(\mu+n+1)}\left((\kappa+1)\mu\frac{P_R}{A_{\kappa\mu}}\right)^{n+\mu} \quad (82)$$

$$\leq \frac{e^{-\frac{\kappa\mu}{2}}}{\Gamma(\mu)\mu}\left((\kappa+1)\mu\frac{P_R}{A_{\kappa\mu}}\right)^{\mu}\sum_{n=1}^{\infty}\frac{1}{n!}\left((\kappa+1)\mu\frac{P_R}{A_{\kappa\mu}}\right)^{n} \quad (83)$$

$$= \tilde{\epsilon}e^{\frac{\kappa\mu}{2}}\left(e^{(\kappa+1)\mu\frac{P_R}{A_{\kappa\mu}}}-1\right), \quad (84)$$

which completes the derivation. In (81) we used the following upper bound [19]:

$$|L_n^{(\alpha)}(x)| \leq \frac{\Gamma(\alpha+n+1)}{n!\Gamma(\alpha+1)}e^{\frac{x}{2}}, \quad (85)$$

and in (82) we used:

$$\frac{\Gamma(\mu+n)}{\Gamma(\mu+n+1)} = \frac{(\mu+n-1)!}{(\mu+n)!} = \frac{1}{\mu+n} \leq \frac{1}{\mu}, \quad (86)$$

for $n \geq 1$.

APPENDIX B
MRC FOR RANDOM VARIABLES WITH POWER-LAW TAILS

A general M-branch MRC PDF solution for independent RV can be obtained through a convolution of the branch PDFs $f_1 * f_2 .. * f_M$, e.g. through the multiplication of moment generating functions and inverse Laplace transform $\mathcal{L}^{-1}$. Approximating the full CDF this way, can result in too complex solutions to readily extract a simple tail approximation. However, it is sufficient to deal with branch tail PDFs only [33]. The lower tail PDF corresponding to (1) can be obtained as:

$$f(P_R) \underset{P_R\to 0}{\approx} \frac{d\alpha\left(\frac{P_R}{A}\right)^\beta}{dP_R} = \alpha\left(\frac{1}{A}\right)^\beta\beta P_R^{\beta-1}. \quad (87)$$

[11] Note that they can be derived separately using similar reasoning.

Using Laplace transform relation [34, ET I 137(1), Table 17.13] $F(s) = \mathcal{L}(f(t)) = 1/s^{\nu} \leftrightarrow f(t) = t^{\nu-1}/\Gamma(\nu)$, the branch $F(s) \approx \alpha \left(\frac{1}{A}\right)^{\beta} \beta \frac{\Gamma(\beta)}{s^{\beta}}$. The i.n.i.d M-branch MRC CDF (for any BPR or β combination), is established as $F_{\mathrm{MRC}}(P_R) = \mathcal{L}^{-1}\left(\frac{1}{s}\prod_{m=1}^{M} F_m(s)\right)$, where $\frac{1}{s}$ is used to produce the CDF from the inverse transform. Using the same Laplace relation as before, we arrive at

$$\epsilon = F_{\mathrm{MRC}}(P_R) \tag{88}$$

$$\approx \mathcal{L}^{-1}\left(\frac{1}{s\prod_{m=1}^{M} s^{\beta_m}}\right) \cdot \prod_{m=1}^{M} \alpha_m \beta_m \frac{\Gamma(\beta_m)}{A_m^{\beta_m}} = \tilde{\epsilon}, \tag{89}$$

which after reordering of terms appears in the form given in (63), completing the derivation.

REFERENCES

[1] P. Popovski, "Ultra-reliable communication in 5G wireless systems," in *Proc. 1st Int. Conf. 5G Ubiquitous Connectivity*, Levi, Finland, Nov. 2014, pp. 146–151.

[2] P. Popovski *et al.*, "Wireless access for ultra-reliable low-latency communication: Principles and building blocks," *IEEE Netw.*, vol. 32, no. 2, pp. 16–23, Mar./Apr. 2018. doi: 10.1109/MNET.2018.1700258.

[3] P. Schulz *et al.*, "Latency critical IoT applications in 5G: Perspective on the design of radio interface and network architecture," *IEEE Commun. Mag.*, vol. 55, no. 2, pp. 70–78, Feb. 2017.

[4] M. Angjelichinoski, K. E. F. Trillingsgaard, and P. Popovski. (2018). "A statistical learning approach to ultra-reliable low latency communication." [Online]. Available: https://arxiv.org/abs/1809.05515

[5] R. Eickhoff, R. Kraemer, I. Santamaria, and L. Gonzalez, "Developing energy-efficient MIMO radios," *IEEE Veh. Technol. Mag.*, vol. 4, no. 1, pp. 34–41, Mar. 2009.

[6] M. Iwabuchi, A. Benjebbour, Y. Kishiyama, and Y. Okumura, "Field experiments on 5G ultra-reliable low-latency communication (URLLC)," *NTT DOCOMO Tech. J.*, vol. 20, no. 1, pp. 14–23, Jul. 2018.

[7] G. D. Durgin, T. S. Rappaport, and D. A. de Wolf, "New analytical models and probability density functions for fading in wireless communications," *IEEE Trans. Commun.*, vol. 50, no. 6, pp. 1005–1015, Jun. 2002.

[8] M. Rao, F. J. Lopez-Martinez, M. S. Alouini, and A. Goldsmith, "MGF approach to the analysis of generalized two-ray fading models," *IEEE Trans. Wireless Commun.*, vol. 14, no. 5, pp. 2548–2561, May 2015.

[9] G. Durisi, T. Koch, and P. Popovski, "Toward massive, ultrareliable, and low-latency wireless communication with short packets," *Proc. IEEE*, vol. 104, no. 9, pp. 1711–1726, Aug. 2016.

[10] *Digital Cellular Telecommunications System (Phase 2+); Radio Transmission and Reception*, Standard TS 145 005 V10.8.0, ETSI, 2014.

[11] J. B. Andersen and I. Z. Kovacs, "Power distributions revisited," in *Proc. COST273 3rd Manage. Committee Meeting*, Jan. 2002, pp. 17–18.

[12] R. Vaughan and J. B. B. Andersen, *Channels, Propagation and Antennas for Mobile Communications*, vol. 50. Michael Faraday House, Stevenage: IET, 2003.

[13] J. Frolik, "On appropriate models for characterizing hyper-Rayleigh fading," *IEEE Trans. Wireless Commun.*, vol. 7, no. 12, pp. 5202–5207, Dec. 2008.

[14] S. A. Saberali and N. C. Beaulieu, "New expressions for TWDP fading statistics," *IEEE Wireless Commun. Lett.*, vol. 2, no. 6, pp. 643–646, Dec. 2013.

[15] A. Bessate and F. El Bouanani, "A very tight approximate results of MRC receivers over independent Weibull fading channels," *Phys. Commun.*, vol. 21, pp. 30–40, Dec. 2016.

[16] M. Nakagami, "The m-distribution—A general formula of intensity of rapid fading," in *Proc. Stat. Methods Radio Wave Propag.*, pp. 3–36, Jun. 1958.

[17] G. J. O. Jameson, "The incomplete gamma functions," *Math. Gazette*, vol. 100, no. 548, pp. 298–306, Jul. 2016.

[18] M. Yacoub, "The $\kappa - \mu$ distribution and the $\eta - \mu$ distribution," *IEEE Antennas Propag. Mag.*, vol. 49, no. 1, pp. 68–81, Feb. 2007.

[19] S. András, Á. Baricz, and Y. Sun, "The generalized Marcum Q—Function: An orthogonal polynomial approach," *Acta Univ. Sapientiae Math.*, vol. 3, no. 1, pp. 60–76, 2011.

[20] S. K. Yoo, S. L. Cotton, P. C. Sofotasios, and S. Freear, "Shadowed fading in indoor off-body communication channels: A statistical characterization using the κ–μ/gamma composite fading model," *IEEE Trans. Wireless Com.*, vol. 15, no. 8, pp. 5231–5244, Aug. 2016.

[21] S. K. Yoo, S. L. Cotton, P. C. Sofotasios, M. Matthaiou, M. Valkama, and G. K. Karagiannidis, "The κ—μ/inverse gamma fading model," in *Proc. IEEE 26th Annu. Int. Symp. Pers., Indoor, Mobile Radio Commun. (PIMRC)*, Aug./Sep. 2015, pp. 425–429.

[22] S. K. Yoo, "Fading wearable communication channels its mitigation," Ph.D. dissertation, Queen Univ. Belfast, Belfast, U.K., 2017. Accessed: Nov. 19, 2017. [Online]. Available: https://pure.qub.ac.uk/portal/files/130797348/thesis_final.pdf

[23] Wolfram Research. *Hypergeometric 1F1*. Assessed: Nov. 19, 2017. [Online]. Available: http://functions.wolfram.com/PDF/Hypergeometric1F1.pdf

[24] J. F. Paris, "Statistical characterization of κ-μ shadowed fading," *IEEE Trans. Veh. Technol.*, vol. 63, no. 2, pp. 518–526, Feb. 2014.

[25] J. Choi and A. K. Rathie, "Certain summation formulas for humbert's double hypergeometric series Ψ_2 and Φ_2," *Commun. Korean Math. Soc.*, vol. 30, no. 4, pp. 439–446, 2015.

[26] M. K. Simon and M.-S. Alouini, *Digital Communication Over Fading Channels*, vol. 95. Hoboken, NJ, USA: Wiley, 2005.

[27] Y. A. Chau and K. Y.-T. Huang, "On the second-order statistics of correlated cascaded Rayleigh fading channels," *Int. J. Antennas Propag.*, vol. 2012, Jun. 2012, Art. no. 108534. [Online]. Available: https://www.hindawi.com/journals/ijap/2012/108534/cta/

[28] H. M. Schöpf and P. H. Supancic, "On Bürmann's theorem and its application to problems of linear and nonlinear heat transfer and diffusion," *Math. J.*, vol. 16, pp. 1–44, Nov. 2014.

[29] S. Winitzki. (2008). *A Handy Approximation for the Error Function and its Inverse*. Assessed: Nov. 19, 2017. [Online]. Available: https://sites.google.com/site/winitzki/sergei-winitzkis-files

[30] V. Plicanic, B. K. Lau, A. Derneryd, and Z. Ying, "Actual diversity performance of a multiband diversity antenna with hand and head effects," *IEEE Trans. Antennas Propag.*, vol. 57, no. 5, pp. 1547–1556, May 2009.

[31] B. R. Yanakiev, J. Ø. Nielsen, M. Christensen, and G. F. Pedersen, "Correlation measurements on small mobile devices," in *Proc. 6th Eur. Conf. Antennas Propag. (EUCAP)*, Mar. 2012, pp. 382–385.

[32] N. A. Johansson, Y.-P. E. Wang, E. Eriksson, and M. Hessler, "Radio access for ultra-reliable and low-latency 5G communications," in *Proc. IEEE Int. Conf. Commun. Workshop (ICCW)*, Jun. 2015, pp. 1184–1189.

[33] P. Hitczenko and S. Montgomery-Smith, "A note on sums of independent random variables," in *Advances in Stochastic Inequalities* (Contemporary Mathematics), T. Hill and C. Houdre, Eds. Providence, RI, USA: A.M.S., 1999, pp. 69–73.

[34] I. Gradshteyn and I. Ryzhik, *Table of Integrals, Series, and Products*, 7th ed. New York, NY, USA: Academic, 2007.

[35] *Study on Scenarios and Requirements for Next Generation Access Technologies*, document TR 38.913 V14.3.0, 3GPP, 2017.

Patrick C. F. Eggers (M'91) was born in Stockholm, Sweden, in 1957. He received the M.Sc.E.E. and Ph.D. degrees from Aalborg University, in 1984 and 2003, respectively. From 1988 to 1989, he was with Telecom New Zealand, where he was involved in multi diffraction path-loss modeling. He is currently an Associate Professor with the Antennas, Propagation and Mm-Wave Systems Section, Aalborg University. He has been responsible for the planning and analysis of propagation work in domestic and EU projects, such as TSUNAMI, CELLO, and i-Rotor. He is the Initiator of the M.Sc.E.E. course at Aalborg University, specializing in wireless communication. He has over 130 publications in journals, conference proceedings, and books. He has 11 filed or granted patents. His research focus is on angular propagation characteristics related to multi-antenna system operation and statistical channel modeling (e.g., ultra-reliable communication), as well as channel characterization in harsh environments relevant for the TETRA system or sensor-based systems with near-field disturbances. He received the Best Paper Award at the IEEE VTC 2007 Fall. He has participated actively in earlier wireless communications related COST actions, starting from COST 207.

Marko Angjelichinoski (S'15) received the Dipl.Ing. and M.Sc. degrees in telecommunications from Sts. Cyril and Methodius University, Skopje, in 2011 and 2014, respectively, and the Ph.D. degree in interplay between the communication, signal processing, and hierarchical control systems in microgrids with high penetration of power electronic converters from Aalborg University, in 2017. He is currently a Post-Doctoral Associate with Duke University. His research interests lie in the broad areas of statistical signal processing, machine learning, and data mining and their applications in various fields, such as communications, power systems, and brain–computer interfaces.

Petar Popovski (S'97–A'98–M'04–SM'10–F'16) received the Dipl.Ing. and Magister Ing. degrees in communication engineering from the University of Sts. Cyril and Methodius, Skopje, and the Ph.D. degree from Aalborg University, in 2005. He is currently a Professor of wireless communications with Aalborg University. He has over 300 publications in journals, conference proceedings, and books. He holds over 30 patents and patent applications. His research interests are in the areas of wireless communication and communication theory. He has served as a Steering Committee Member for the IEEE INTERNET OF THINGS JOURNAL. He is currently a Steering Committee Member of the IEEE SmartGridComm and the IEEE TRANSACTIONS ON GREEN COMMUNICATIONS AND NETWORKING. He received the ERC Consolidator Grant in 2015, the Danish Elite Researcher Award in 2016, the IEEE Fred W. Ellersick Prize in 2016, and the IEEE Stephen O. Rice prize in 2018. He is featured in the list of Highly Cited Researchers 2018, compiled by Web of Science. He is also the General Chair for the IEEE SmartGridComm 2018 and the IEEE Communication Theory Workshop 2019. He is also an Area Editor of the IEEE TRANSACTIONS ON WIRELESS COMMUNICATIONS.